



This is a repository copy of *A dynamic model of air-breathing polymer electrolyte fuel cell (PEFC): A parametric study.*

White Rose Research Online URL for this paper:  
<https://eprints.whiterose.ac.uk/174383/>

Version: Accepted Version

---

**Article:**

Calili, F., Ismail, M.S. [orcid.org/0000-0002-9539-8925](https://orcid.org/0000-0002-9539-8925), Ingham, D.B. [orcid.org/0000-0002-4633-0852](https://orcid.org/0000-0002-4633-0852) et al. (3 more authors) (2021) A dynamic model of air-breathing polymer electrolyte fuel cell (PEFC): A parametric study. *International Journal of Hydrogen Energy*, 46 (33). pp. 17343-17357. ISSN 0360-3199

<https://doi.org/10.1016/j.ijhydene.2021.02.133>

---

Article available under the terms of the CC-BY-NC-ND licence  
(<https://creativecommons.org/licenses/by-nc-nd/4.0/>).

**Reuse**

This article is distributed under the terms of the Creative Commons Attribution-NonCommercial-NoDerivs (CC BY-NC-ND) licence. This licence only allows you to download this work and share it with others as long as you credit the authors, but you can't change the article in any way or use it commercially. More information and the full terms of the licence here: <https://creativecommons.org/licenses/>

**Takedown**

If you consider content in White Rose Research Online to be in breach of UK law, please notify us by emailing [eprints@whiterose.ac.uk](mailto:eprints@whiterose.ac.uk) including the URL of the record and the reason for the withdrawal request.



[eprints@whiterose.ac.uk](mailto:eprints@whiterose.ac.uk)  
<https://eprints.whiterose.ac.uk/>

1 **A Dynamic Model of Air-breathing Polymer Electrolyte Fuel Cell (PEFC):**  
2 **A Parametric Study**

3 F. Calili <sup>a,b</sup>, M. S. Ismail <sup>a, c\*</sup>, D.B. Ingham <sup>a</sup>, K. J. Hughes <sup>a</sup>, L. Ma <sup>a</sup>, M. Pourkashanian <sup>a, c</sup>

4 <sup>a</sup> Energy 2050, Department of Mechanical Engineering, Faculty of Engineering, University of  
5 Sheffield, Sheffield, S3 7RD, Sheffield. United Kingdom.

6 <sup>b</sup> Department of Energy Systems Engineering, Iskenderun Technical University, Hatay 31  
7 200, Turkey

8 <sup>c</sup> Translational Energy Research Centre, University of Sheffield, Sheffield S3 7RD, United  
9 Kingdom

10  
11 \*Corresponding author

12 Tel: +44 114 215 7244

13 Email address:

14 [m.s.ismail@sheffield.ac.uk](mailto:m.s.ismail@sheffield.ac.uk) (M. S. Ismail)

1 **Abstract**

2 A dynamic model for an air-breathing PEFC has been built to investigate the transient response  
3 of the fuel cell to load changes. The sensitivities of the dynamic response, as well as the steady  
4 state performance, to: the ambient temperature and relative humidity; the thickness and the  
5 thermal conductivity of the cathode GDL; and the fuel utilisation, have been studied. A  
6 previously-developed steady-state model of the fuel cell was linked to the dynamic model to  
7 feed the latter with the data of the cell temperature as it changes with the current density. It was  
8 found that, when there are sudden changes to high loads, there exist optimum values for the  
9 ambient temperature and GDL thickness at which the overshoots are mitigated and the steady  
10 state performance is improved. Further, the transient and steady state performance were found  
11 to improve with increasing the ambient relative humidity and GDL thermal conductivity.  
12 Finally, the fuel utilisation was found to have no impact on the dynamic response of the fuel  
13 cell. All the above findings have been presented and discussed in the paper.

14 **Keywords:** Air-breathing PEFCs; Dynamic model; Transient response; Load changes

15

16

# 1. Introduction

Portable electronic devices, such as smartphones and laptops, have become an increasingly essential part of our daily life. In this huge market, power demand is growing fast. Portable polymer electrolyte fuel cells (PEFCs) are strong candidates to act as an alternative power source for small electronic devices due to their appealing features: long charge cycle (i.e. of the order of a few days), high efficiency and grid-independence [1]–[5]. The cathode of portable PEFCs is typically open to the ambient in order to directly extract (by natural convection): (i) oxygen required for the completion of the electrochemical reaction and (ii) water vapour required for the initial humidification of the polymeric membrane. Thus, PEFCs, with an open cathode, do not require an air/oxygen storage device and humidifier, thus simplifying the fuel cell system. This type of PEFCs is normally described as air-breathing PEFCs.

Since oxygen is passively supplied from the ambient air by natural convection, the performance of air-breathing PEFCs is sensitive to the ambient conditions. Particularly, liquid water formation at the open porous cathode is strongly affected by the ambient conditions. Some models and experimental studies that investigated the impact of ambient conditions on the performance of air-breathing PEFCs are presented in the following paragraphs.

Rajani and Kolar [6] investigated the effect of various sets of ambient conditions (20-80% ambient relative humidity and 10-40 °C ambient temperature) on the performance of the air-breathing PEFC using a two-dimensional, single phase, non-isothermal and steady-state numerical model. They concluded that the ambient temperature dominantly affects the fuel cell performance compared to relative humidity of the ambient. Matamoros and Brüggemann [7] developed a three-dimensional and non-isothermal model to observe how different ambient conditions influence the concentration and ohmic losses in air-breathing PEFCs. They

1 demonstrated that concentration losses were more dominant than ohmic losses on the  
2 performance of the air-breathing PEFC at different ambient conditions. Chen et al. [8] built a  
3 zero-dimensional mathematical model to investigate the impact of hydrogen relative humidity  
4 on the performance of air-breathing PEFCs at ambient temperatures of 10, 20 and 30°C. It was  
5 found that the limiting current density increases with increasing hydrogen relative humidity.  
6 Ismail et al. [9] developed a zero-dimensional mathematical model for an air-breathing PEFC.  
7 They found that a high ambient relative humidity with a low ambient temperature is  
8 advantageous at low cell potential while a low ambient relative humidity with a moderate  
9 ambient temperature is favourable at intermediate fuel cell potentials.

10 Hottinen et al. [10] and Fabian et al. [11] experimentally investigated the effects of ambient  
11 temperatures and relative humidities on the performance of air-breathing fuel cells using  
12 environmental chambers. Hottinen et al. [10] found that the air-breathing PEFC displayed the  
13 best performance at low ambient temperatures where the temperature gradient between the  
14 open cathode of the fuel cell and the ambient region is a maximum. Fabian et al. [11] showed  
15 that the maximum power density was achieved at an ambient temperature of 20°C and a relative  
16 humidity of 40%. Jeong et al. [12] also used an environmental chamber and showed that the  
17 cell performance at low current densities could be enhanced with increasing the ambient  
18 relative humidity from 20 to 100%. Chun et al. [13] improved heat dissipation of the air-  
19 breathing PEFC using thin-fin structures in the open cathode design. In a later work [14], the  
20 same research group investigated the effects of fin structures at different ambient temperatures  
21 (30°C, 40°C and 50°C).

22 The characteristics of cathode gas diffusion layer (GDL) also play a significant role in  
23 managing the water balance within the air-breathing PEFC. O'Hayre et al. [15] developed a  
24 non-isothermal, one-dimensional numerical model and investigated the impact of GDL

1 characteristics (i.e. GDL thickness and thermal conductivity) on an air-breathing PEFC. They  
2 showed that GDL thickness should be optimised to provide an adequate balance between heat  
3 and mass transfers, thus maximising the performance of the air-breathing fuel cell. Jeong et al.  
4 [16] reported that the performance of air-breathing PEFC was enhanced with increasing the  
5 GDL thickness from 100 to 280  $\mu\text{m}$ ; increasing the GDL thickness beyond 280  $\mu\text{m}$  was found  
6 to adversely affect the fuel cell performance. Furthermore, the effects of the wettability of the  
7 GDL [17]–[20] and the material and the structure of the GDL [21]–[24] on the performance of  
8 air-breathing PEFCs have been also investigated.

9 The power demand of portable devices may significantly change with time. For instance, the  
10 power demand of a smartphone may suddenly and/or significantly change as a result of the use  
11 of multiple power-demanding applications. Hence, one of the main challenges is to make the  
12 air-breathing PEFCs as highly responsive as possible to the rapid and/or large load changes in  
13 the small electronic device.

14 MATLAB/Simulink software is often used to create dynamic models for fuel cell-based  
15 systems. Several researches have been performed to understand the dynamic characteristics of  
16 different types of fuel cells used in various applications with an ultimate aim of improving their  
17 load following abilities. Padulles et al. [25] proposed a dynamic model for power systems  
18 incorporating solid oxide fuel cells and described some modelling methodologies of the fuel  
19 cell stack and the power conditioner. They demonstrated that the dynamic model is an effective  
20 tool to determine the safe and durable operating conditions in a solid oxide fuel cell power  
21 plant. El-Sharkh et al. [26] proposed a dynamic model for a direct methanol fuel cell power  
22 plant used for residential applications and studied its transient under various load changes; they  
23 tested the model using an actual residential load profile for a period of 4 h and concluded that  
24 the dynamic model of the fuel cell power plant exhibits a good conformity. Uzunoglu and

1 Alam [27] designed a grid-independent system for residential applications that comprises of a  
2 PEFC plant and an ultracapacitor-based storage unit that supplies extra power during peak  
3 periods. They created a dynamic model for the system and their results showed that the  
4 combination of the above units improves the overall performance of the system and decreases  
5 the size and the cost of the PEFC unit. In a later work [28], they investigated the dynamic  
6 behaviour of the PEFC power plant operating in parallel with a battery bank to power different  
7 loads: a washing machine, a microwave, computers, transformers and a resistive load bank.  
8 The experimental data were used to validate the output of the dynamic model. They concluded  
9 that the PEFC power plant requires an extra energy storage device, such as a battery bank, to  
10 assist the PEFC during large load transients. Yalcinoz [29] proposed a dynamic model of  
11 PEFCs used to power electric bicycles. Many researchers have designed different types of  
12 controllers to improve the dynamic response of the conventional fuel cells by particularly  
13 controlling input gases flowrates such as micro-chip [30] and fuzzy logic controllers [31]–[34].  
14 Morner and Klein [35] experimentally studied the dynamic behaviour of a PEFC stack to  
15 investigate the effects of humidity, temperature and air-flowrate on the transient response of  
16 the fuel cell. Unlike conventional PEFCs, there was only one study on the dynamic response  
17 of air-breathing PEFCs in the literature [36]; Yalcinoz and Alam [36] developed, using  
18 MATLAB/Simulink, a dynamic model for an air-breathing PEFC and validated it against the  
19 modelling data at an ambient temperature of 10 °C and relative humidity of 40% reported by  
20 O’Hayre et al. [15]. The above model was then integrated into a larger-in-scale dynamic model  
21 for a system powering a laptop. Notably, Yalcinoz and Alam [36] run their model for a single  
22 set of conditions and parameters.

23 In this study, a dynamic model for an air-breathing PEFC is developed to investigate, for the  
24 first time, the effects of the ambient conditions (temperature and relative humidity), GDL

1 parameters (thickness and thermal conductivity) and fuel (i.e. hydrogen) utilisation on the  
2 transient response of the fuel cell to rapid and large load alterations. Further, a previously-  
3 developed steady-state model of the fuel cell was linked to the dynamic model to provide the  
4 latter with the data representing the changes of temperature with the current density. This is an  
5 attempt to better understand the factors that may affect the response of the air-breathing fuel  
6 cells to load changes and how to improve this response.

## 7 **2. Air-breathing PEFC Model**

### 8 *2.1 Model characteristics and assumptions*

9 The dynamic model of a single air-breathing PEFC used in this study is developed within the  
10 platform of MATLAB/Simulink. The modelled fuel cell was originally fabricated and reported  
11 by Fabian et al. [11]; the geometry and the physical parameters of the fuel cell are listed in  
12 Table 1. The dynamics of the fuel cell model are expressed in the Laplace domain. The dynamic  
13 model consists of three main subsystems: Nernst voltage, activation losses and ohmic losses  
14 (Fig. 1). The mass concentration losses are not considered in this model as the sharp decline in  
15 the cell voltage at high current densities of the modelled fuel cell was found to be due to the  
16 increased membrane resistance induced by the exponential increase in cell temperature at these  
17 high current densities [9], [11], [15]. The subsystem “Cell Temperature” shown in Fig. 1 links  
18 the dynamic model with a steady-state model for the fuel cell that was developed in an earlier  
19 work [9]; namely, the steady-state model was used to feed the dynamic model with the surface  
20 temperature of the cathode GDL of the fuel cell (or simply cell temperature as the temperature  
21 difference across the components of the PEFC is relatively small, i.e.  $\leq 2^{\circ}\text{C}$ ) as it changes with  
22 current density (more details are available in the introduction of Section 3). It should be noted  
23 that the details of the steady-state model were not included in the present in order not to distract

1 the flow of the present work whose main theme is the transient response of the air-breathing  
2 PEFCs; the interested reader is referred to [9] for further details about the steady-state model.  
3 The outputs of the dynamic model are the fuel cell voltage and power and below are the  
4 assumptions and considerations that have been employed for the model [11].

5 (i) Water exists only in vapour form.

6 (ii) Gases are assumed to be ideal.

7 (iii) The anode of the fuel cell is in dead-end mode and the fuel used is dry.

8 (iv) The water activity is uniform through the membrane and is in equilibrium with water  
9 vapour activity in the cathode catalyst layer.

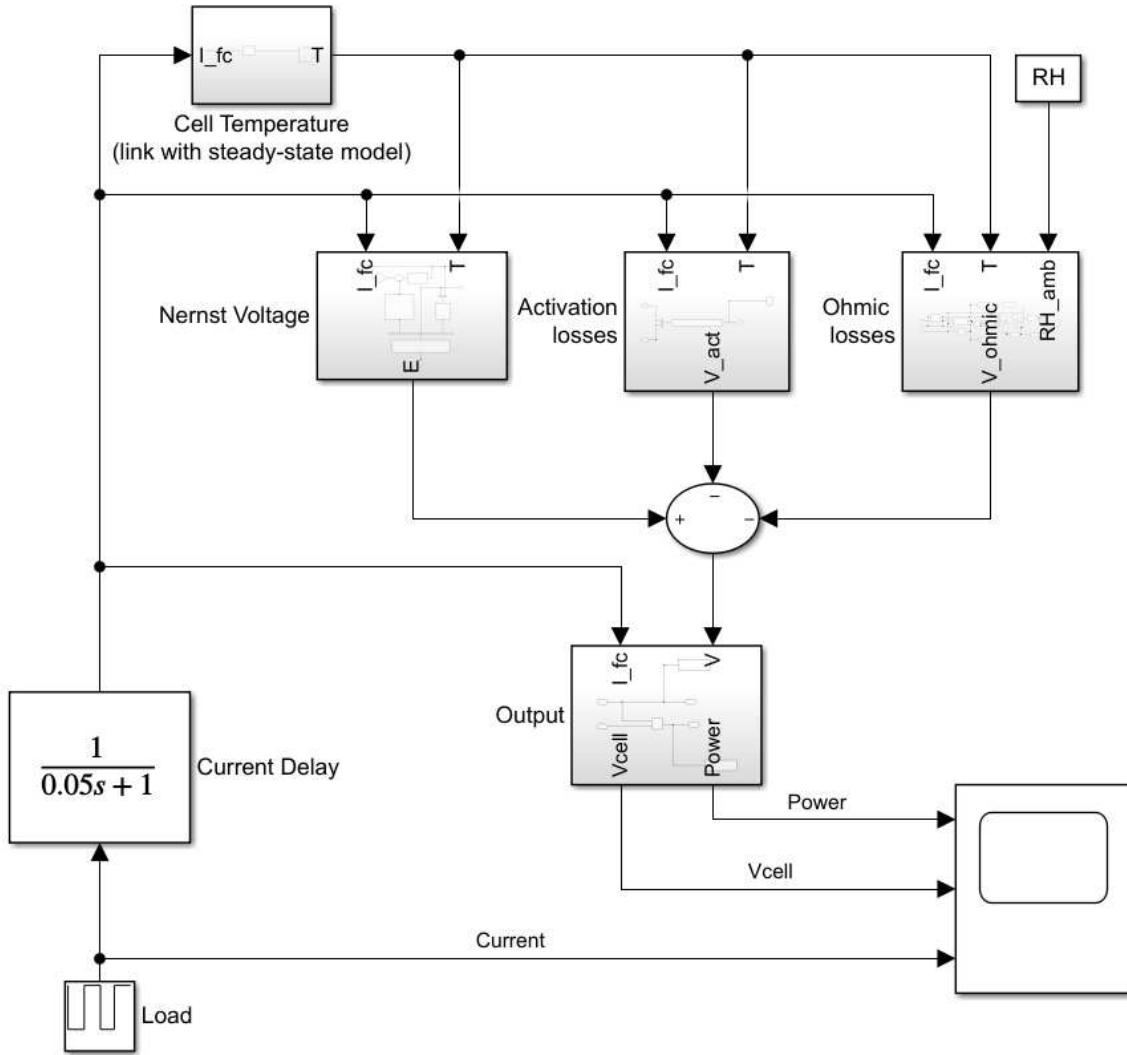
10 (v) The cathode catalyst layer is infinitely thin so that it could be treated as an interface between  
11 the membrane and the cathode GDL.

12 (vi) The lengths of the fuel cell channels are small (i.e. 3 cm) and therefore the variation of  
13 pressure along the channel could be ignored [25].

14 It should be noted that Fabian et al. [11] found that some water accumulates at the cathode of  
15 the fuel cell, particularly at the intermediate current densities for certain operating conditions  
16 (low temperatures and high relative humidity). However, as the running air-breathing fuel cell  
17 was of high-performance, liquid water accumulation starts to diminish as the current density  
18 increases and this is due to the exponential increase of the cell temperature at such high current  
19 densities. Under the latter conditions, the sharp decline in the cell potential at high current  
20 densities is primarily due to membrane dehydration, not water flooding.

21 It is appreciated that accounting for water flooding in the steady-state model (originally  
22 developed by Ismail et al. [9]) linked to the dynamic model will make the outcomes of the latter

1 model more accurate. However, as water flooding may only occur in the intermediate current  
 2 densities of the modelled fuel cell and has therefore no significant impact on the overall trends  
 3 of the outcomes of the model, we assume that, for simplification, water only exists as a vapour;  
 4 O’Hayre et al. [15] and Ismail et al. [9] considered the same assumption.



5

6

Fig. 1. The block diagram of the air-breathing PEFC dynamic model.

7 **2.2 Calculation of Cell Voltage**

8 The proportional relationship between the hydrogen molar flow through a valve and its partial  
 9 pressure inside the flow channel can be stated as follows [26], [31]:

$$\frac{q_{H_2}}{P_{H_2}} = K_{H_2} \quad (1)$$

1

2 where  $q_{H_2}$  is the molar flow rate of hydrogen,  $P_{H_2}$  is the partial pressure of hydrogen and  $K_{H_2}$   
 3 is the molar valve constant for hydrogen.

4 The partial pressure of hydrogen is obtained using the ideal gas law:

$$P_{H_2} V_{an} = n_{H_2} RT \quad (2)$$

5 where  $V_{an}$  is the volume of the anode compartment [25],  $n_{H_2}$  is the number of hydrogen moles  
 6 in the anode channel,  $R$  is the universal gas constant and  $T$  is the absolute temperature.

7 The derivation of Eq. (2) with respect to time gives:

$$\frac{d}{dt} P_{H_2} = \frac{RT}{V_{an}} q_{H_2} \quad (3)$$

8 The molar flow rate of hydrogen can be calculated using the following expression:

$$q_{H_2} = q_{H_2}^{in} - q_{H_2}^{out} - q_{H_2}^r \quad (4)$$

9 where  $q_{H_2}^{in}$  is the inlet flow rate of hydrogen,  $q_{H_2}^{out}$  is the outlet flow rate of hydrogen and  $q_{H_2}^r$   
 10 is the flow rate of reacting hydrogen.

11 According to Faraday's second law of electrolysis, the molar flow rate of reacting hydrogen  
 12 can be expressed as a function of the fuel cell current  $I$ :

$$q_{H_2}^r = \frac{I}{2F} \quad (5)$$

13 where  $F$  is the Faraday's constant. Substituting Eq. (4) and Eq. (5) into Eq. (3) gives:

$$\frac{d}{dt} P_{H_2} = \frac{RT}{V_{an}} \left( q_{H_2}^{in} - q_{H_2}^{out} - \frac{I}{2F} \right) \quad (6)$$

1 After replacing the output hydrogen flow given by Eq. (1) into Eq. (6), the partial pressure of  
 2 the hydrogen can be determined in the Laplace domain as [25]–[28], [31], [37]:

$$P_{H_2} = \frac{1/K_{H_2}}{1 + \tau_{H_2}s} \left( q_{H_2}^{in} - \frac{I}{2F} \right) \quad (7)$$

3 where  $\tau_{H_2}$  is hydrogen time constant and given by:

$$\tau_{H_2} = \frac{V_{an}}{K_{H_2}RT} \quad (8)$$

4 and the derivation of Eq. (7) is given in Appendix A. The partial pressure of the oxygen,  $P_{O_2}$ ,  
 5 in the open cathode compartment is given by [36]:

$$P_{O_2} = x_{O_2}P = x_{O_2}^0 - L_{GDL} \frac{jRT}{4FD_{O_2}^{eff}} \quad (9)$$

6 where  $x_{O_2}^0$  is the mole fraction of the oxygen in the ambient (i.e. 0.21),  $L_{GDL}$  is the GDL  
 7 thickness,  $j$  is the current density,  $P$  is the ambient pressure (i.e. 1 atm) and  $D_{O_2}^{eff}$  is the effective  
 8 diffusivity of oxygen into air given by:

$$D_{O_2}^{eff} = \frac{\varepsilon}{\tau} D_{O_2,air} \quad (10)$$

9 where  $D_{O_2,air}$  is the binary diffusivity of oxygen into air and  $\varepsilon$  and  $\tau$  are the GDL porosity and  
 10 tortuosity, respectively.

11 The reversible (or Nernst) voltage of the fuel cell ( $E$ ) is obtained using Nernst equation [38]:

$$E = E_0 + \frac{RT}{2F} \ln(P_{H_2} \cdot P_{O_2}^{1/2}) \quad (11)$$

12 where  $E_0$  represents the standard reversible fuel cell voltage (i.e. 1.23 V). The block diagram  
 13 of the Nernst voltage is shown in Fig. 2.

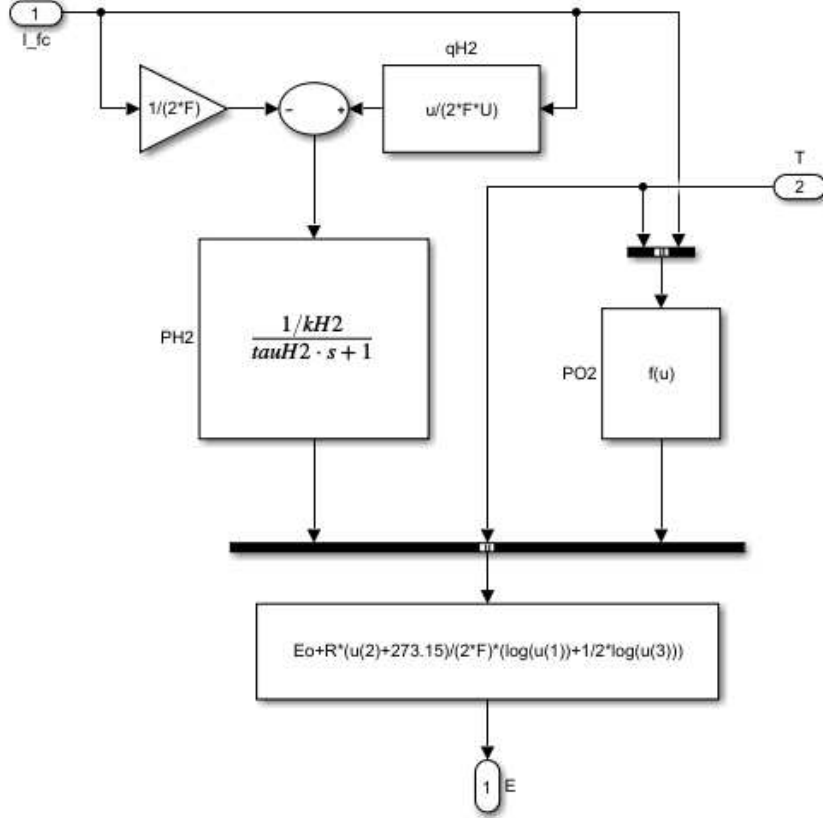


Fig. 2. The block diagram of the Nernst voltage.

The activation losses,  $\eta_{act}$ , are obtained using the equation [36]:

$$\eta_{act} = \frac{RT}{2\alpha F} \ln\left(\frac{j}{j_0}\right) \quad (12)$$

where  $\alpha$  is the charge transfer coefficient and  $j_0$  is the reference exchange current density, which can be corrected for temperature by the following expression:

$$j_0 = j_{303K}^0 \exp\left[\frac{E_a}{R}\left(\frac{1}{303} - \frac{1}{T}\right)\right] \quad (13)$$

where  $E_a$  is the activation energy for the oxygen reduction reaction. The ohmic losses,  $\eta_{ohmic}$ , can be calculated as follows [9]:

$$\eta_{ohmic} = jA_{act}(R_{elec} + R_{mem}) \quad (14)$$

where  $A_{act}$  is the active area of the fuel cell,  $R_{elec}$  represents the lumped electrical resistance of the cell and  $R_{mem}$  is the membrane resistance and is defined as follows:

$$R_{mem} = \frac{L_{mem}}{A_{act}\sigma_{mem}} \quad (15)$$

1 where  $L_{mem}$  is the thickness of the Nafion<sup>®</sup> membrane and  $\sigma_{mem}$  represents the ionic  
2 conductivity of the membrane which is given by [39]:

$$\sigma_{mem} = (3.46a^3 + 0.0161a^2 + 1.45a - 0.175) \exp\left[1268\left(\frac{1}{303} - \frac{1}{T}\right)\right] \quad (16)$$

3 The water activity  $a$  in Eq. (16) is defined as follows [38]:

$$a = \frac{P_{H_2O}}{P_{sat}} \quad (17)$$

4 where  $P_{H_2O}$  and  $P_{sat}$  are respectively the partial pressure and saturation pressure of water  
5 vapour at the fuel cell temperature.  $P_{sat}$  is obtained by [40]:

$$\log_{10}P_{sat} = -2.1794 + 0.02953(T - 273.15) - 9.1837 \times 10^{-5}(T - 273.15)^2 + 1.4454 \times 10^{-7}(T - 273.15)^3 \quad (18)$$

6 A similar equation to Eq. (9) can be used to calculate the partial pressure of water vapour:

$$P_{H_2O} = x_{H_2O}P = x_{H_2O}^0 + L_{GDL} \frac{jRT}{2FD_{H_2O}^{eff}} \quad (19)$$

7

$$x_{H_2O}^0 = \frac{RH \times P_{sat}}{100} \quad (20)$$

8 where  $x_{H_2O}^0$  is the mole fraction of the water vapour in the ambient, RH is the ambient relative  
9 humidity and  $D_{H_2O}^{eff}$  is the effective diffusivity of water into air and is given by:

$$D_{H_2O}^{eff} = \frac{\varepsilon}{\tau} D_{H_2O,air} \quad (21)$$

10 Having calculated the Nernst voltage (Eq. (11)), the activation losses (Eq. (12)) and ohmic  
11 losses (Eq. (14)), the cell potential of the air-breathing PEFC,  $V_{cell}$ , could be then calculated:

$$V_{cell} = E - \eta_{act} - \eta_{ohmic} \quad (22)$$

1 The concentration losses have not been taken into account in the model as the factors that cause  
2 them were always found to be rather insignificant in our simulation: the water activity was  
3 always less than unity, thus signalling that there was no liquid water saturation and there was  
4 always abundance of reactant gasses available for the reaction even at high current densities.

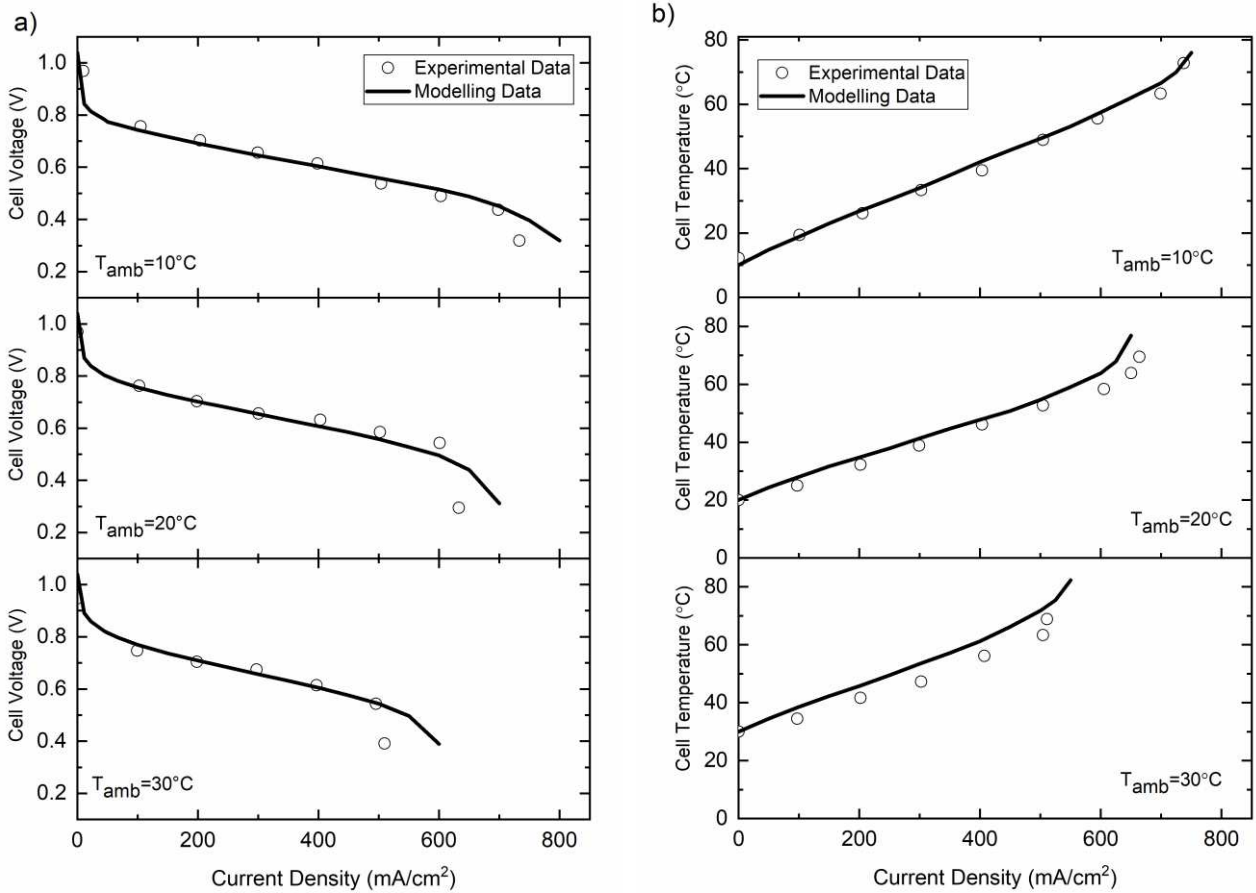
5 Table 1 Parameters in the air-breathing PEFC dynamic model ([11], [15], [36]).

Parameters	Value
Universal gas constant, $R$	8.3145 J/(mol.K)
Faraday's constant, $F$	96500 C/mol
Standard reversible fuel cell voltage, $E_0$	1.23 V
Ambient pressure, $P$	1 atm
Binary diffusivity of $O_2$ in air, $D_{O_2,air}$	$2.1 \times 10^{-5} \text{ m}^2/\text{s}$
Binary diffusivity of $H_2O$ in air, $D_{H_2O,air}$	$2.6 \times 10^{-5} \text{ m}^2/\text{s}$
Length of active cell side (square), $L_a$	0.03 m
Cell active area, $A_{act}$	$0.0009 \text{ m}^2$
Membrane thickness, $L_{mem}$	$5.2 \times 10^{-5} \text{ m}$
GDL thickness, $L_{GDL}$	$3.0 \times 10^{-4} \text{ m}$
GDL porosity, $\varepsilon$	0.4
GDL tortuosity, $\tau$	3.0
GDL thermal conductivity, $k_{GDL}$	10 W/(m.K)
Activation energy, $E_a$	50 kJ/mol
Reference exchange current density, $j_{303K}^0$	$5 \times 10^{-5} \text{ A}/\text{cm}^2$
Lumped cell electrical resistance, $R_{elec}$	12 m $\Omega$
Charge transfer coefficient, $\alpha$	0.28
Utilization factor, $U$	0.7
Hydrogen time constant, $\tau_{H_2}$	0.3096 s
Hydrogen valve constant, $K_{H_2}$	$3.627 \times 10^{-5} \text{ mol}/(\text{s. atm})$

6

### 1 **3. Model Validation**

2 The air-breathing PEFC dynamic model is validated against the experimental data reported by  
3 Fabian et al. [11]. Fig. 3a shows the polarisation curves generated by the model (when reaching  
4 steady state conditions) at an ambient relative humidity of 40% and ambient temperatures of  
5 10, 20 and 30°C. The results are in a good agreement with the corresponding experimental  
6 polarisation curves, and moreover, the decline in the fuel cell performance with increasing  
7 ambient temperature is well captured by the fuel cell model. It is noteworthy that the only  
8 fitting parameter in the model is the reference exchange current density. The data showing the  
9 variation of the surface temperature of the open cathode with the current density of the fuel cell  
10 for the set of variables investigated in this study (i.e. the ambient conditions of temperature and  
11 relative humidity, the thickness and the thermal conductivity of the cathode GDL and hydrogen  
12 utilisation) was generated from a steady-state model developed and reported in a previous work  
13 [9]. The above data were fitted using high order polynomials and directly linked to the dynamic  
14 model; Appendix B presents some example polynomials. Fig. 3b shows that the model (after  
15 reaching steady state conditions) predicts well the change of the surface temperature with  
16 ambient temperature and current density. In particular, the sharp increases in the GDL surface  
17 temperature at high current densities are captured well by the model. Such good agreements  
18 between the outputs of the model and the experimental data over a wide range of ambient  
19 temperatures impart a high degree of confidence in the prediction abilities of the developed  
20 model.



1 Fig. 3. Modelling and experimental data for an air-breathing PEFC operating under an ambient RH of 40% and  
 2 ambient temperatures of 10,20 and 30 °C: a) the polarisation curves and b) the cell temperature of the cathode  
 3 GDL as a function of current density.

#### 4. Results and Discussion

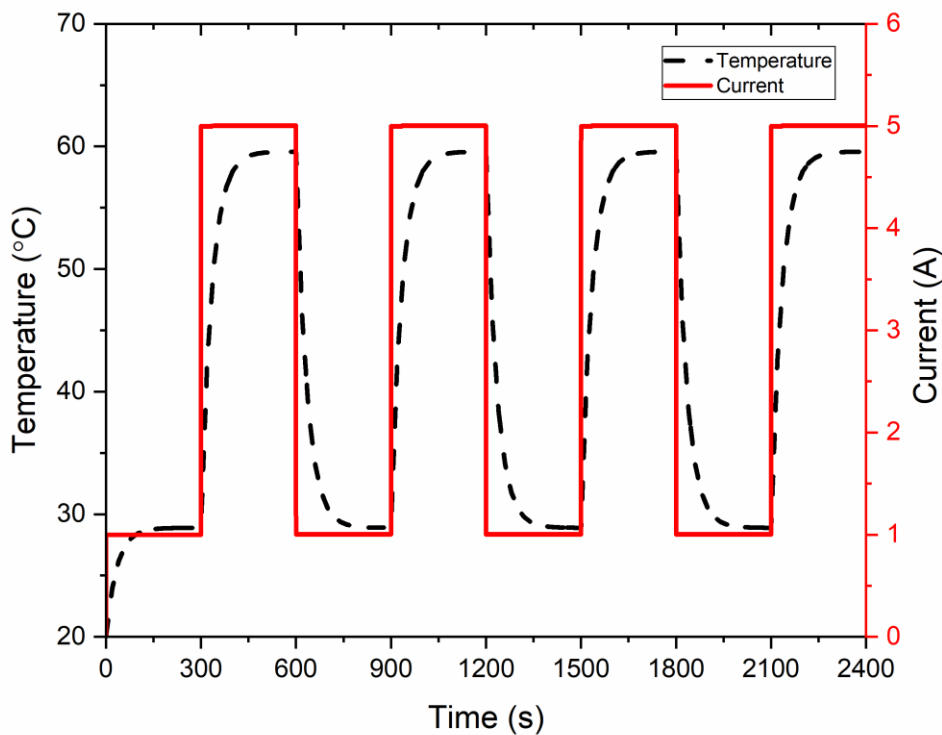
##### 4.1 Transient Operation

6 The current was, using the “Repeating Sequence Stairs” built-in function in Simulink,  
 7 programmed to rapidly change between low (i.e. 1 A) and high (i.e. 5 A) values after each 300  
 8 s for 2400 s; 300 s was experimentally found to be sufficient for the potential of the air-  
 9 breathing fuel cell to stabilise [11]. The evolution of the fuel cell temperature with time was  
 10 modelled by Kim et al.[41]:

$$T(t) = T_2 + (T_1 - T_2) \times \exp(-0.0295t) \quad (23)$$

1 where  $T_1$  is the steady cell temperature before applying the current step change and  $T_2$  is the  
 2 steady cell temperature after applying the step change. Note that both  $T_1$  and  $T_2$  are provided  
 3 by the steady-state model linked to the dynamic model as described in Section 3.

4 Fig. 4 demonstrates that the fuel cell current alternates between 1 and 5 A under ambient  
 5 conditions of 40% relative humidity and 20°C. It can be seen that the step change of the current  
 6 causes the fuel cell temperature to sharply increase/decrease before starting to stabilise after  
 7 around 100 s of the step change.



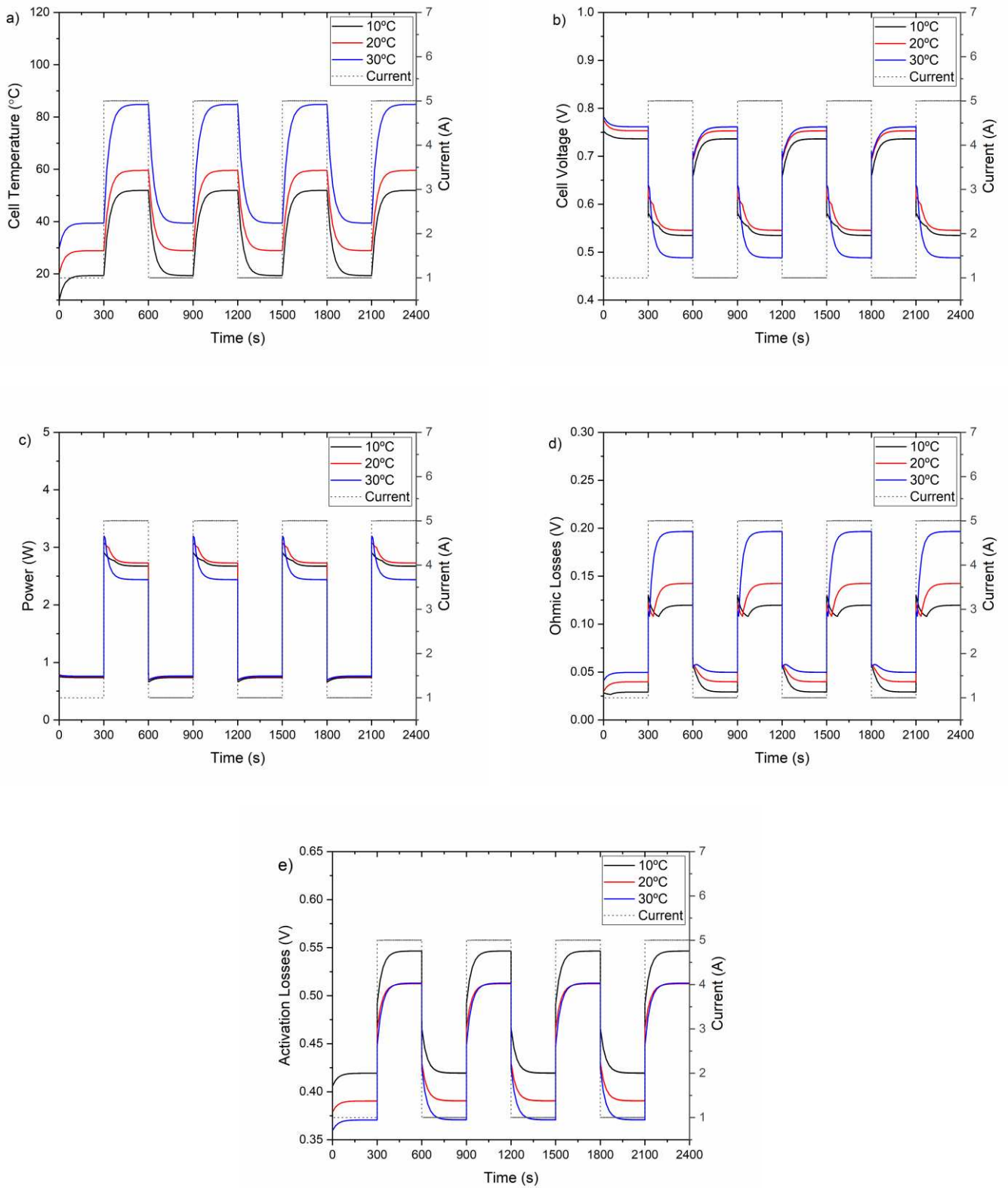
8

9 Fig. 4. The fuel cell temperature as it changes with alternating 4-A step changes in the fuel cell current under  
 10 ambient conditions of 40% RH and 20°C.

## 1 *4.2 Effect of Ambient Temperature*

2 Fig. 5 shows the effects of the ambient temperature on the dynamic behaviour and the  
3 performance of the fuel cell for a given ambient relative humidity of 40%. The figure shows  
4 there exists an optimum ambient temperature at which the fuel cell performance is maximised,  
5 i.e. 20°C. The activation and ohmic losses at this ambient temperature are of reasonable values.  
6 On the other hand, a relatively high ambient temperature (i.e. 30°C) causes an increase in fuel  
7 cell temperature (Fig. 5a) and an exponential increases in the saturation pressure of the water  
8 vapour, thus decreasing the water content and ionic conductivity of the membrane phase and  
9 ultimately increasing the ohmic losses (Fig. 5d). This also causes the output power of the fuel  
10 cell to have an increased overshoot when changing to a high current step (Fig. 5c). It is  
11 noteworthy that the overshoots in the output power of the fuel cell that occur as a result of the  
12 current step changes are similar to those obtained by Uzunoglu and Alam [27]. On the other  
13 hand, a relatively low ambient temperature (i.e. 10°C) results in less ohmic losses but higher  
14 activation losses compared to those of 20°C ambient temperature.

15 Fig. 5d shows that, when changing to a high current step, the ohmic losses start to decrease and  
16 then increase with different rates for different ambient temperatures before stabilisation. This  
17 is attributed to the two-field effect of the temperature as evident from Equations (16-18).  
18 Namely, as the current is increased to 5 A, the cell temperature increases causing an initial  
19 increase in the ionic conductivity of the membrane phase (Eq. (16)). However, as time passes,  
20 this positive effect of the cell temperature on the ionic conductivity is outweighed by the  
21 exponential increase in the saturation pressure of the water vapour with increasing temperature  
22 (Eq. (18)) which eventually leads to a decrease in the water content and the ionic conductivity  
23 of the membrane phase before reaching the steady state values.

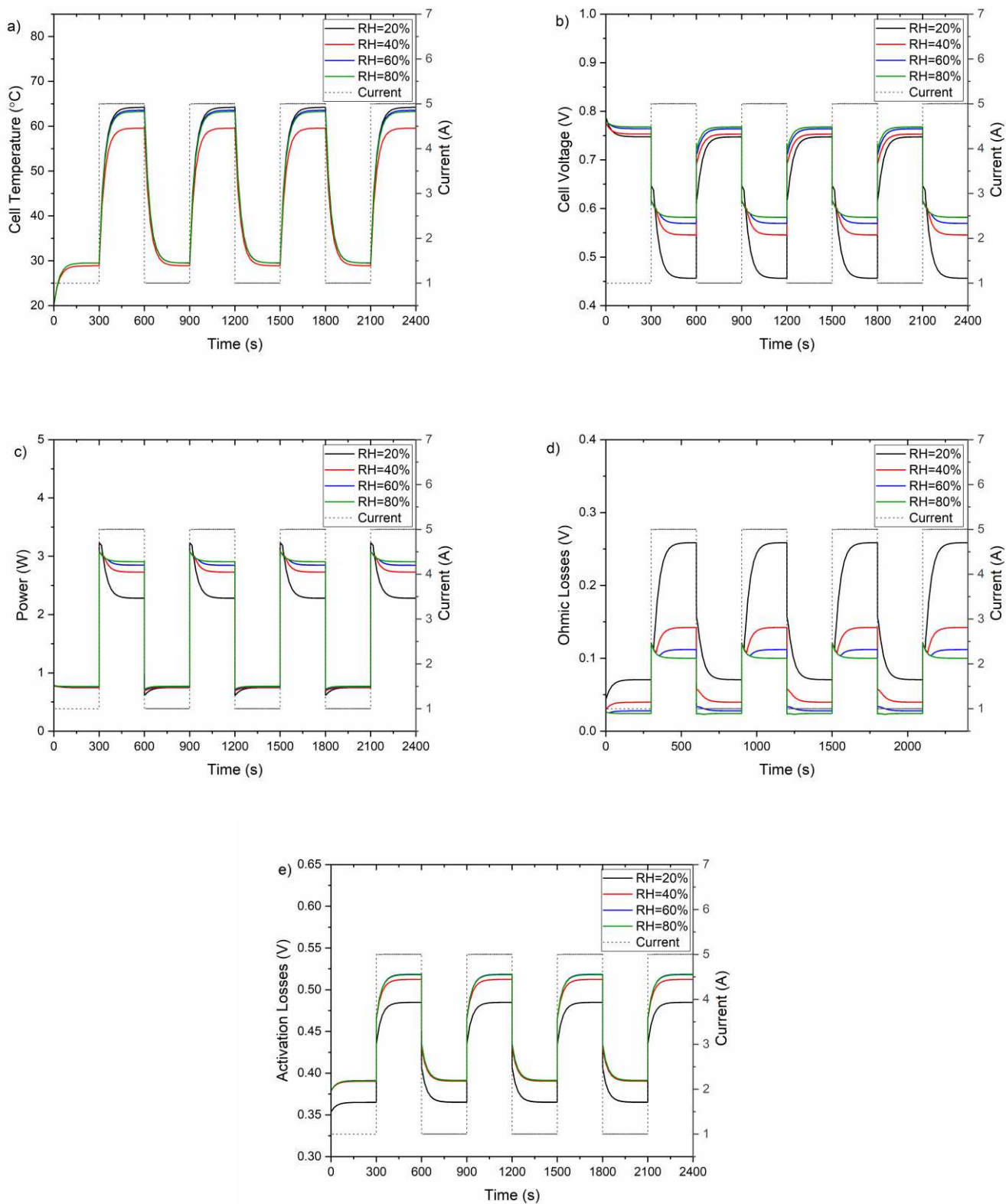


1 Fig. 5. Transient profiles for: a) cell temperature, b) voltage, c) output power, d) ohmic losses and e) activation  
 2 losses of air-breathing PEFC under different values for the ambient temperature and a constant ambient relative  
 3 humidity of 40%.

### 1 ***4.3 Effect of Ambient Relative Humidity***

2 Fig. 6 shows the effect of the ambient relative humidity on the dynamic behaviour and the  
3 performance of the fuel cell for a given ambient temperature of 20°C. The fuel cell temperature  
4 is lowest with an ambient relative humidity of 40% (Fig. 6a); this could be attributed to the  
5 heat sources: the product of the current density and each one of the ohmic losses and the  
6 activation losses. Namely, the ohmic losses with 40% relative humidity are less than those with  
7 20% relative humidity (Fig. 6d) and this is due to better membrane hydration with 40% relative  
8 humidity. Equally, the activation losses with 40% relative humidity are less than those with 60  
9 and 80% relative humidities (Fig. 6e) and this is due to less current densities demonstrated by  
10 the former case (i.e. 40% relative humidity). Such combined effects of activation and ohmic  
11 losses result in 40% relative humidity case having the lowest cell temperature.

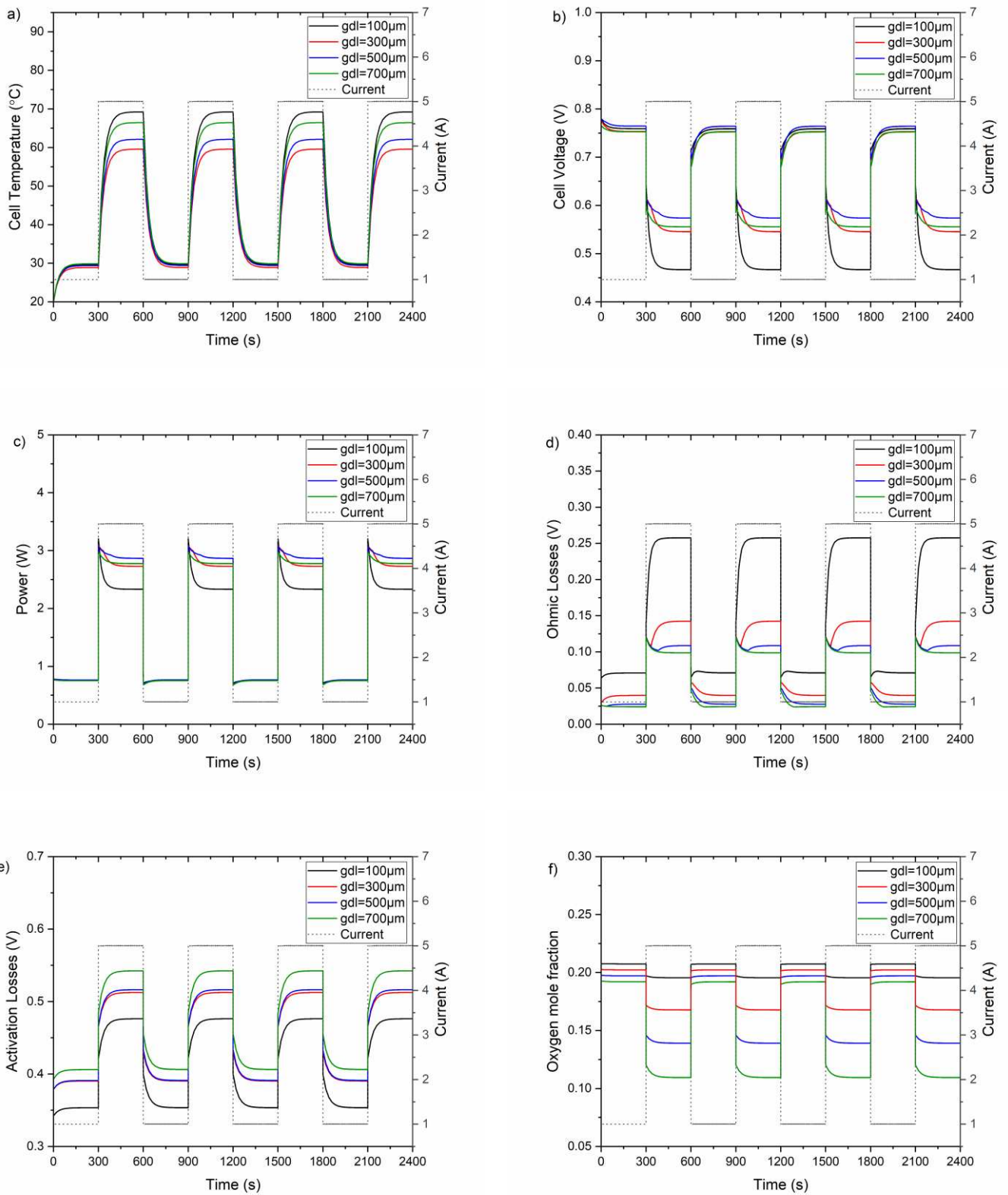
12 Apart from 40% RH, the temperature profile of the fuel cell at 1 A is almost the same for the  
13 ambient relative humidities of 20, 60 and 80%, while at 5A the temperature slightly decreases  
14 with increasing relative humidity from 20 to 80%. Fig. 6b and Fig. 6c show that, when changing  
15 to a high current step, the overshoot is a maximum with the lowest relative humidity (i.e. 20%),  
16 especially at high current intervals, and this is due to the increased ionic resistance, caused by  
17 membrane dry-out, at this low RH; this is evident from the ohmic losses profiles shown in Fig.  
18 6d. On the other hand, the overshoots become less profound with increasing ambient relative  
19 humidity and this is more apparent at high current intervals where the fuel cell is more ohmic  
20 losses limited; this signals that the well-hydrated membrane enhances the dynamic behaviour  
21 of the air-breathing PEFC.



1 Fig. 6. Transient profiles for: a) cell temperature, b) voltage, c) output power, d) ohmic losses and e) activation  
 2 losses of air-breathing PEFC under different values for the ambient relative humidity and a constant ambient  
 3 temperature of 20°C.

#### 1 ***4.4 Effect of GDL Thickness***

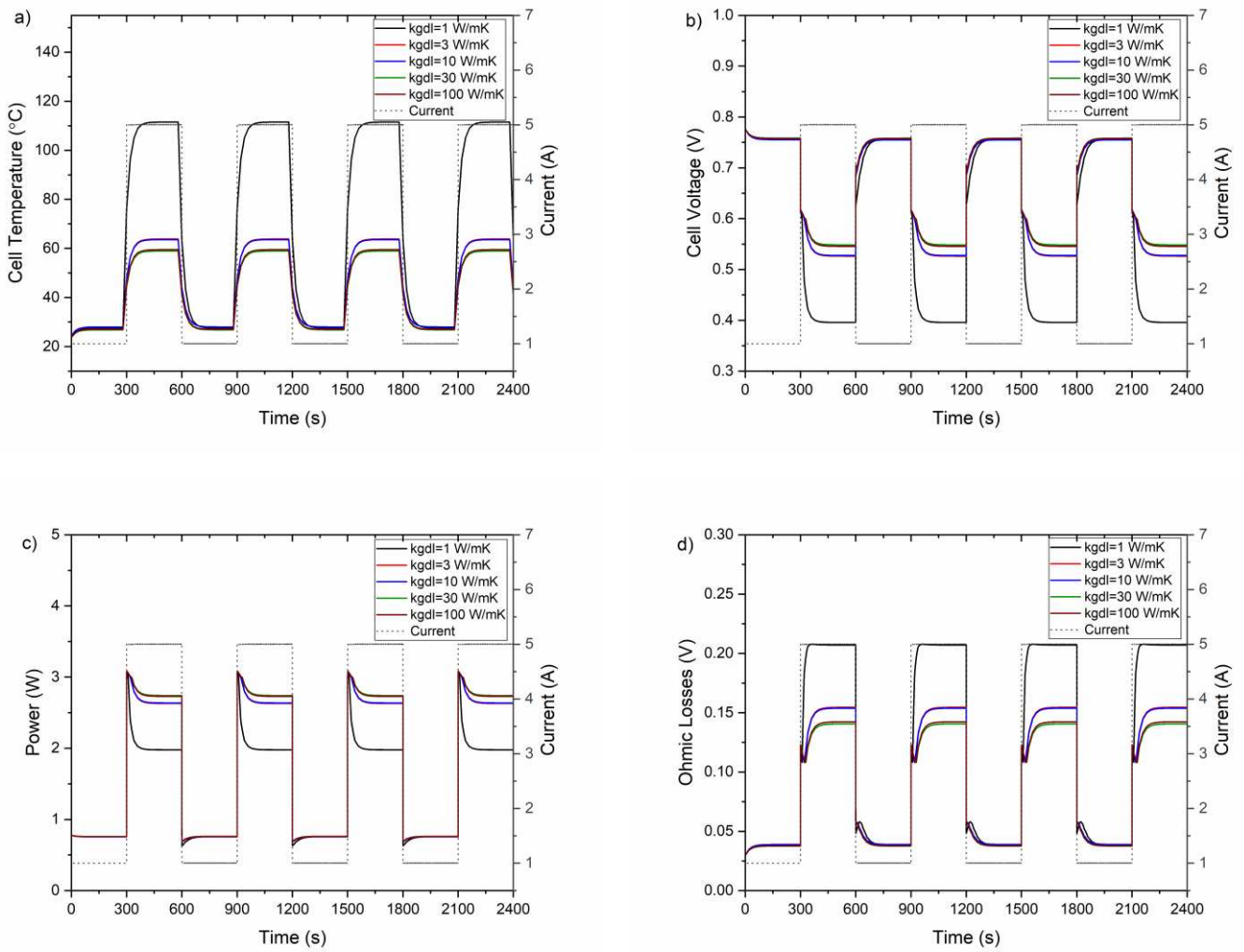
2 Fig. 7 shows the effects of the cathode GDL thickness on the dynamic behaviour and the  
3 performance of the fuel cell for given ambient conditions of 20°C and 40% RH. Overall, the  
4 figure shows that there exists an optimum GDL thickness at which the dynamic response and  
5 the performance of the fuel cell are maximised: 500 µm. This thickness provides a good balance  
6 between the ohmic and activation losses; see Fig. 7(d-e). Too thin GDL (i.e. 100 µm) ensures  
7 a fast supply of oxygen to the catalyst layer (Fig. 7f) and subsequently the decrease in the  
8 activation losses (Fig. 7e). However, this too thin GDL (compared to other thicknesses) allows  
9 for more transfer of the produced water (required to humidify the membrane phase) from the  
10 cathode catalyst layer to the ambient; this leads to a lower ionic conductivity, increased ohmic  
11 losses (Fig. 7d) and a high overshoot (Fig. 7c). On the other hand, too thick GDL (i.e. 700 µm)  
12 increases the mass transport resistance, leading to: (i) more produced water being available for  
13 membrane humidification, higher ionic conductivity and less ohmic losses (Fig. 7d) and (ii)  
14 less oxygen being available for the reaction at the cathode catalyst layer (Fig. 7f), and higher  
15 activation losses (Fig. 7e). The transient temperature profile (Fig. 7a) shows a slightly different  
16 trend: the lowest surface temperature is demonstrated by not the 500 µm thick GDL but by the  
17 300 µm thick GDL and this is attributed to the shorter thermal pathway of the latter GDL. The  
18 highest surface temperature is featured by the 100 µm thick GDL and this is due to the  
19 substantial ohmic losses demonstrated by this GDL. It should be noted that, due to the higher  
20 consumption of oxygen and production of water rates, all the above effects are significantly  
21 more profound at high current steps (i.e. 5 A). The above results reveal that the GDL thickness  
22 should be optimized to ensure obtaining reasonable values for the activation (through  
23 increasing the supply rate of oxygen to the catalyst layer) and ohmic (through decreasing the  
24 rejection rate of produced water required for humidification of membrane phase) losses.



1 Fig. 7. Transient profiles for: a) cell temperature, b) voltage, c) output power, d) ohmic losses, e) activation losses  
 2 and f) oxygen mole fraction of the air breathing PEFC under a variety of GDL thicknesses for the ambient  
 3 conditions of 20 $^{\circ}\text{C}$  and 40% relative humidity.

#### 1 ***4.5 Effect of GDL Thermal Conductivity***

2 Fig. 8 shows the effects of cathode GDL thermal conductivity on the dynamic behaviour and  
3 the performance of the fuel cell for given ambient conditions of 20°C and 40% RH. As with  
4 [15], the base value of the GDL thermal conductivity is 10 W/(m.K). The 1-100 W/(m.K)  
5 range was selected to cover a variety of materials that could be possibly used for the GDLs:  
6 the metal-based GDLs whose thermal conductivity is of the order 100 W/(m.K) and  
7 conventional GDLs whose carbon fibres are mainly oriented in the transverse directions (1  
8 W/(m.K)) [42], [43]. The figure shows that the fuel cell performance becomes better as the  
9 GDL thermal conductivity increases. The transient behaviour also shows significantly less  
10 overshoot with higher thermal conductivities (Fig. 8c). Nonetheless, the fuel cell demonstrates  
11 an asymptotic behaviour with increasing GDL thermal conductivity; no performance gain is  
12 obtained with a thermal conductivity higher than 30 W/(m.K). On the other hand, extremely  
13 low thermal conductivity (i.e. 1 W/(m.K)) significantly lowers the fuel cell performance and  
14 incurs a substantial overshoot when abruptly changing to a high current step. Such a low  
15 thermal conductivity significantly decreases the dissipation rate of heat and subsequently  
16 increases the fuel cell temperature (Fig. 8a), exponentially increases the saturation pressure of  
17 water, decreases the water content and ionic conductivity of the membrane phase and  
18 ultimately significantly increases the ohmic losses (Fig. 8d). It should be noted that the effects  
19 of the thermal conductivity are indirectly taken into account through the cell temperature-  
20 current density data generated by the steady-state model linked to the dynamic model.

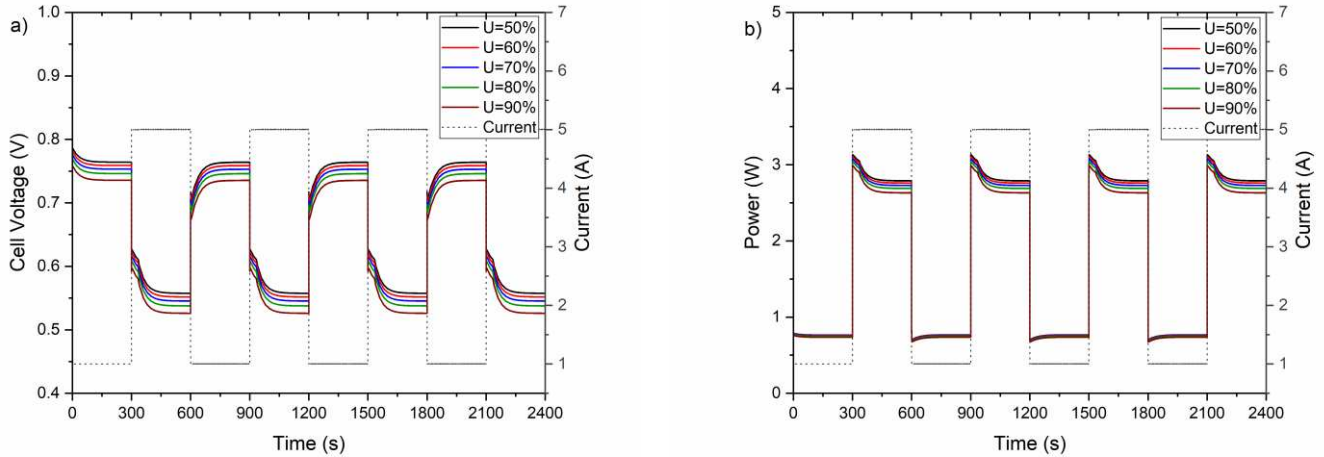


1 Fig. 8. Transient profiles for: a) cell temperature, b) voltage, c) output power and d) ohmic losses of the air  
 2 breathing PEFC under a variety of GDL thermal conductivity for the ambient conditions of 20°C and 40% relative  
 3 humidity.

#### 4 **4.6 Effect of Hydrogen Utilisation**

5 Fig. 9 shows the effects of the hydrogen utilisation (i.e. the portion of the supplied fuel that is  
 6 consumed in the reaction) on the dynamic behaviour and the performance of the fuel cell for  
 7 given ambient conditions of 20°C and 40% RH. It was found that the hydrogen utilisation has  
 8 no effect on the activation and ohmic losses (not shown) and consequently no impact on the  
 9 dynamic behaviour of the fuel cell. However, the figure shows that the fuel cell performance  
 10 improves with decreasing hydrogen utilisation. As the hydrogen utilisation decreases, a higher

- 1 hydrogen flow rate is provided, thus increasing the partial pressure of hydrogen and
- 2 subsequently the Nernst voltage of the fuel cell (Eq. (11)).



3 Fig. 9. Transient profiles for: a) voltage and b) output power of the air breathing PEFC under a variety of values of  
 4 hydrogen utilisation for the ambient conditions of 20°C and 40% relative humidity.

## 5. Conclusions

6 A dynamic model has been developed for an air-breathing PEFC to analyse its transient  
 7 response to load changes and explore the sensitivity of this response to the ambient conditions,  
 8 GDL parameters and hydrogen utilisation. A previously developed steady-state model for the  
 9 fuel cell was directly linked to the dynamic model to provide the latter with the data of the fuel  
 10 cell temperature changing with the current density. The following are the key findings of the  
 11 study:

- 12 • Relatively high ambient temperature and low ambient relative humidity result in  
 13 significant overshoots when changing from low load (1 A) to high load (5 A) and this  
 14 is due to the substantial increase in the ohmic losses, caused by the membrane dry-out,  
 15 under the above ambient conditions. 20°C was found to be the optimum ambient  
 16 temperature at which the fuel cell demonstrates less overshoot and better steady state

1 performance as a good balance between the activation and the ohmic losses is achieved  
2 at this ambient temperature. On the other hand, the transient and the steady state  
3 performances of the fuel cell were found to be improve with increasing relative  
4 humidity due to the same reasons mentioned for the optimum temperature of 20°C.

- 5 • The cathode GDL thickness requires to be optimised to ensure reasonable transient and  
6 steady state cell performances; it was found to be 500  $\mu\text{m}$  in this study. Too thin GDL  
7 (e.g. 100  $\mu\text{m}$ ) increases the supply rate of oxygen to the catalyst layer but at the same  
8 time increases the rejection rate of water required for the humidification of the  
9 membrane phase, thus resulting in high ohmic losses, significant overshoot and poor  
10 performance when changing to a high load. On the other hand, too thick GDL (e.g. 700  
11  $\mu\text{m}$ ) ensures a good retention of water required for the membrane humidification but  
12 impacts on the transport rate of oxygen to the catalyst layer.
- 13 • The thermal conductivity of the cathode GDL requires to be reasonably high (e.g.  $\sim 30$   
14  $\text{W}/(\text{m}\cdot\text{K})$ ). Extremely low thermal conductivity (e.g.  $1 \text{ W}/(\text{m}\cdot\text{K})$ ) hinders the rate of  
15 heat dissipation, thus leading to an unacceptable decrease in the ionic conductivity of  
16 the membrane phase and a subsequent increase in the ohmic losses that ultimately  
17 results in a high overshoot and poor performance. On the other hand, no performance  
18 gain was observed beyond a GDL thermal conductivity of  $30 \text{ W}/(\text{m}\cdot\text{K})$ .
- 19 • Hydrogen utilisation has no effect on the dynamic response of the fuel cell to the load  
20 changes. However, as it decreases, the fuel cell performance becomes slightly better as  
21 the amount of hydrogen supplied to the anodic compartment increases, increasing the  
22 partial pressure of hydrogen and subsequently the theoretical open circuit voltage (i.e.  
23 Nernst voltage) of the fuel cell. However, hydrogen utilisation is typically aimed to be  
24 maximised in order to save the fuel cost.

# 1 Nomenclature

## 2 Roman symbols

$a$	Water activity [-]
$A_{act}$	Active area of the fuel cell [ $m^2$ ]
$D_{H_2O}^{eff}$	Effective diffusivity of water into air [ $m^2/s$ ]
$D_{H_2O,air}$	Binary diffusivity of water into air [ $m^2/s$ ]
$D_{O_2}^{eff}$	Effective diffusivity of oxygen into air [ $m^2/s$ ]
$D_{O_2,air}$	Binary diffusivity of oxygen into air [ $m^2/s$ ]
$E$	Nernst Voltage [V]
$E_a$	Activation energy [J/mol]
$E_0$	Standard fuel cell voltage [V]
$F$	Faraday's constant [C/mol]
$j$	Current density [ $A/m^2$ ]
$j_0$	Reference exchange current density [ $A/m^2$ ]
$I$	Electric current [A]
$k_{GDL}$	GDL Thermal conductivity [W/(m. K)]
$K_{H_2}$	Hydrogen valve constant [mol/(atm. s)]
$L_{GDL}$	GDL thickness [m]
$L_{mem}$	Membrane thickness [m]
$n_{H_2}$	Number of hydrogen moles
$P$	Ambient pressure[atm]
$P_{H_2}$	Partial pressure of hydrogen [atm]
$P_{H_2O}$	Partial pressure of water vapour [atm]
$P_{sat}$	Water vapour saturation pressure [atm]
$P_{O_2}$	Partial pressure of oxygen [atm]
$q_{H_2}$	Hydrogen molar flow [mol/s]
$R$	Universal Gas Constant [atm/(mol. K)]
$RH$	Relative humidity [%]
$R_{elec}$	Lumped electrical cell resistance [ $\Omega$ ]
$R_{mem}$	Membrane resistance [ $\Omega$ ]
$T$	Absolute temperature [K]
$U$	Utilization factor [-]
$V_{an}$	Anode volume [ $m^3$ ]

$V_{cell}$	Cell voltage [V]
$x$	Mole fraction [–]

### 1 *Greek symbols*

$\alpha$	Charge transfer coefficient [–]
$\varepsilon$	Porosity [–]
$\eta_{act}$	Activation over voltage [V]
$\eta_{ohmic}$	Ohmic over voltage [V]
$\sigma_{mem}$	Ionic conductivity [S/m]
$\tau$	Tortuosity [–]
$\tau_{H_2}$	Hydrogen time constant [s]

2

### 3 **Acknowledgements**

4 Fatma Calili thanks the Ministry of National Education at the Republic of Turkey for funding  
5 her PhD studentship at the University of Sheffield.

### 6 **Appendix A: Derivation of Eq. (7)**

7 Partial pressure of hydrogen flow in Laplace domain (Eq. (7)) can be derived by following  
8 steps:

$$q_{H_2}^{out} = K_{H_2} \cdot P_{H_2} \quad (A.1)$$

9 Substituting Eq. (A.1) into Eq. (6):

$$\frac{d}{dt} P_{H_2} = \frac{RT}{V_{an}} (q_{H_2}^{in} - K_{H_2} \cdot P_{H_2} - \frac{I}{2F}) \quad (A.2)$$

10 In Laplace domain:

$$\mathcal{L}(P_{H_2}(t)) = P_{H_2}(s) \quad (A.3)$$

$$\mathcal{L}\left(\frac{d}{dt} P_{H_2}(t)\right) = sP_{H_2}(s) \quad (A.4)$$

11 Substituting Eq. (A.3) and Eq. (A.4) into Eq. (25):

$$sP_{H_2}(s) = \frac{RT}{V_{an}}(q_{H_2}^{in} - K_{H_2} \cdot P_{H_2}(s) - \frac{I}{2F}) \quad (A.5)$$

1  $P_{H_2}(s)$  can be determined as follows:

$$P_{H_2}(s) = \frac{1/K_{H_2}}{1 + \frac{V_{an}}{K_{H_2}RT}s} (q_{H_2}^{in} - \frac{I}{2F}) \quad (A.6)$$

2 where  $\frac{V_{an}}{K_{H_2}RT}$  is hydrogen time constant,  $\tau_{H_2}$  (Eq. (8)) and final form of the partial pressure of hydrogen

3 flow in Laplace domain is given by:

$$P_{H_2}(s) = \frac{1/K_{H_2}}{1 + \tau_{H_2}s} (q_{H_2}^{in} - \frac{I}{2F}) \quad (A.7)$$

4

## 5 **Appendix B: Fuel cell temperature as a function current density**

6 The fuel cell temperature is obtained using the following general form polynomial fitted using

7 the data generated by a code developed by Ismail et al. [9]:

$$T = a_1 \cdot j^7 + a_2 \cdot j^6 + a_3 \cdot j^5 + a_4 \cdot j^4 + a_5 \cdot j^3 + a_6 \cdot j^2 + a_7 \cdot j + a_8 \quad (24)$$

8 where  $T$  is the cathode GDL surface temperature and  $j$  is the current density.  $a_1, a_2 \dots a_8$  are

9 coefficients given in Table B.

10 Table B Values of coefficient in Eq. (B.1) at different ambient temperatures and an ambient relative humidity of  
11 40%.

<i>Coefficients</i>	10°C	20°C	30°C
$a_1$	$2.51 \times 10^{-24}$	$7.02 \times 10^{-24}$	$1.93 \times 10^{-23}$
$a_2$	$-6.37 \times 10^{-20}$	$-1.52 \times 10^{-19}$	$-3.46 \times 10^{-19}$
$a_3$	$6.34 \times 10^{-16}$	$1.30 \times 10^{-15}$	$2.43 \times 10^{-15}$
$a_4$	$-3.13 \times 10^{-12}$	$-5.50 \times 10^{-12}$	$-8.49 \times 10^{-12}$
$a_5$	$8.07 \times 10^{-9}$	$1.20 \times 10^{-8}$	$1.54 \times 10^{-8}$
$a_6$	$-1.04 \times 10^{-5}$	$-1.31 \times 10^{-5}$	$-1.39 \times 10^{-5}$
$a_7$	$1.36 \times 10^{-2}$	$1.39 \times 10^{-2}$	$1.34 \times 10^{-2}$
$a_8$	282.94	292.92	302.93

12

## 1 **References**

- 2 [1] Ferreira-Aparicio P, Conde JJ, Chaparro AM. Fundamentals and components of  
3 portable hydrogen fuel-cell systems. In: Ferreira-Aparicio P, Chaparro AM, editors.  
4 Portable Hydrogen Energy Systems, San Diego: Academic Press Inc; 2018, p. 15-39.  
5 <https://doi.org/10.1016/B978-0-12-813128-2.00002-4>
- 6 [2] Wilberforce T, Alaswad A, Palumbo A, Dassisti M, Olabi AG. Advances in stationary  
7 and portable fuel cell applications. Int J Hydrogen Energy 2016;41(37):16509-22.  
8 <https://doi.org/10.1016/j.ijhydene.2016.02.057>
- 9 [3] Giddey S, Badwal SP, Ciacchi FT, Fini D, Sexton BA, Glenn F, et al. Investigations  
10 on fabrication and lifetime performance of self-air breathing direct hydrogen micro  
11 fuel cells. Int J Hydrogen Energy 2010;35(6):2506-16.  
12 <https://doi.org/10.1016/j.ijhydene.2009.12.158>
- 13 [4] Zhang Y, Mawardi A, Pitchumani R. Numerical studies on an air-breathing proton  
14 exchange membrane (PEM) fuel cell stack. J Power Sources 2007;173(1):264-76.  
15 <https://doi.org/10.1016/j.jpowsour.2007.05.008>
- 16 [5] Litster S, Pharoah JG, McLean G, Djilali N. Computational analysis of heat and mass  
17 transfer in a micro-structured PEMFC cathode. J Power Sources 2006;156(2):334-44.  
18 <https://doi.org/10.1016/j.jpowsour.2005.05.064>
- 19 [6] Rajani BP, Kolar AK. A model for a vertical planar air breathing PEM fuel cell. J  
20 Power Sources 2007;164(1):210-21. <https://doi.org/10.1016/j.jpowsour.2006.10.055>
- 21 [7] Matamoros L, Brüggemann D. Concentration and ohmic losses in free-breathing  
22 PEMFC. J Power Sources 2007;173(1):367-74.  
23 <https://doi.org/10.1016/j.jpowsour.2007.02.091>

- 1 [8] Chen Z, Ingham D, Ismail M, Ma L, Hughes KJ, Pourkashanian M. Effects of  
2 hydrogen relative humidity on the performance of an air-breathing PEM fuel cell. Int J  
3 Numer Methods Heat Fluid Flow 2019. <https://doi.org/10.1108/HFF-11-2018-0674>
- 4 [9] Ismail MS, Ingham DB, Hughes KJ, Ma L, Pourkashanian M. An efficient  
5 mathematical model for air-breathing PEM fuel cells. Appl Energy 2014;135:490-503.  
6 <https://doi.org/10.1016/j.apenergy.2014.08.113>
- 7 [10] Hottinen T, Nojonen M, Mennola T, Himanen O, Mikkola M, Lund P. Effect of  
8 ambient conditions on performance and current distribution of a polymer electrolyte  
9 membrane fuel cell. J Appl Electrochem 2003;33(3-4):265-71.  
10 <https://doi.org/10.1023/A:1024184824662>
- 11 [11] Fabian T, Posner JD, O'Hayre R, Cha SW, Eaton JK, Prinz FB, et al. The role of  
12 ambient conditions on the performance of a planar, air-breathing hydrogen PEM fuel  
13 cell. J Power Sources 2006;161(1):168-82.  
14 <https://doi.org/10.1016/j.jpowsour.2006.03.054>
- 15 [12] Jeong SU, Cho EA, Kim HJ, Lim TH, Oh IH, Kim SH. Effects of cathode open area  
16 and relative humidity on the performance of air-breathing polymer electrolyte  
17 membrane fuel cells. J Power Sources 2006;158(1):348-53.  
18 <https://doi.org/10.1016/j.jpowsour.2005.09.044>
- 19 [13] Chun D, Kim D, Williamson ZR, Lee T, Squibb CW. Investigation of fin based  
20 oxygen supply modules on the performance of air-breathing polymer electrolyte  
21 membrane fuel cells. Appl Therm Eng 2013;50(1):293-301.  
22 <https://doi.org/10.1016/j.applthermaleng.2012.06.039>
- 23 [14] Williamson ZR, Chun D, Kwon K, Lee T, Squibb CW, Kim D. Evaluation of fin

- 1 structure effects on a heated air-breathing polymer electrolyte membrane (PEM) fuel  
2 cell. *Appl Therm Eng* 2013;56(1-2):54-61.  
3 <https://doi.org/10.1016/j.applthermaleng.2013.02.036>
- 4 [15] O'Hayre R, Fabian T, Litster S, Prinz FB, Santiago JG. Engineering model of a  
5 passive planar air breathing fuel cell cathode. *J Power Sources* 2007;167(1):118-29.  
6 <https://doi.org/10.1016/j.jpowsour.2007.01.073>
- 7 [16] Jeong SU, Cho EA, Kim HJ, Lim TH, Oh IH, Kim SH. A study on cathode structure  
8 and water transport in air-breathing PEM fuel cells. *J Power Sources*  
9 2006;159(2):1089-94. <https://doi.org/10.1016/j.jpowsour.2005.12.046>
- 10 [17] Fu Y, Hou M, Xu H, Hou Z, Ming P, Shao Z, et al. Ag–polytetrafluoroethylene  
11 composite coating on stainless steel as bipolar plate of proton exchange membrane fuel  
12 cell. *J Power Sources* 2008;182(2):580-4.  
13 <https://doi.org/10.1016/j.jpowsour.2008.04.051>
- 14 [18] Baroutaji A, Carton JG, Oladoye AM, Stokes J, Twomey B, Olabi AG. Ex-situ  
15 evaluation of PTFE coated metals in a proton exchange membrane fuel cell  
16 environment. *Surf Coatings Technol* 2017;323:10-7.  
17 <https://doi.org/10.1016/j.surfcoat.2016.11.105>
- 18 [19] Carton JG, Lawlor V, Olabi AG, Hochenauer C, Zauner G. Water droplet  
19 accumulation and motion in PEM (Proton Exchange Membrane) fuel cell mini-  
20 channels. *Energy* 2012;39(1):63-73. <https://doi.org/10.1016/j.energy.2011.10.023>
- 21 [20] Schmitz A, Tranitz M, Eccarius S, Weil A, Hebling C. Influence of cathode opening  
22 size and wetting properties of diffusion layers on the performance of air-breathing  
23 PEMFCs. *J Power Sources* 2006;154(2):437-47.

- 1 <https://doi.org/10.1016/j.jpowsour.2005.10.070>
- 2 [21] Baroutaji A, Carton JG, Stokes J, Olabi AG. Application of open pore cellular foam  
3 for air breathing PEM fuel cell. Int J Hydrogen Energy 2017;42(40):25630-8.  
4 <https://doi.org/10.1016/j.ijhydene.2017.05.114>
- 5 [22] Hottinen T, Himanen O, Lund P. Effect of cathode structure on planar free-breathing  
6 PEMFC. J Power Sources 2004;138(1-2):205-10.  
7 <https://doi.org/10.1016/j.jpowsour.2004.06.044>
- 8 [23] Liao S, Dang D, Tian X, Hou S, Liu F, Peng H, et al. Enhanced water management in  
9 the cathode of an air-breathing PEMFC using a dual catalyst layer and optimizing the  
10 gas diffusion and microporous layers. Int J Hydrogen Energy 2015;40(10):3961-7.  
11 <https://doi.org/10.1016/j.ijhydene.2015.01.091>
- 12 [24] Ferreira-Aparicio P, Chaparro AM. Influence of the cathode architecture in the  
13 frequency response of self-breathing proton exchange membrane fuel cells. J Power  
14 Sources 2014;272:79-89. <https://doi.org/10.1016/j.jpowsour.2014.08.046>
- 15 [25] Padulles J, Ault GW, McDonald JR. An integrated SOFC plant dynamic model for  
16 power systems simulation. J Power Sources 2000;86(1-2):495-500.  
17 [https://doi.org/10.1016/S0378-7753\(99\)00430-9](https://doi.org/10.1016/S0378-7753(99)00430-9)
- 18 [26] El-Sharkh MY, Rahman A, Alam MS, Byrne PC, Sakla AA, Thomas T. A dynamic  
19 model for a stand-alone PEM fuel cell power plant for residential applications. J Power  
20 Sources 2004;138(1-2):199-204. <https://doi.org/10.1016/j.jpowsour.2004.06.037>
- 21 [27] Uzunoglu M, Alam MS. Dynamic modeling, design, and simulation of a combined  
22 PEM fuel cell and ultracapacitor system for stand-alone residential applications. IEEE

- 1 Trans Energy Convers 2006;21(3):767-75. [10.1109/TEC.2006.875468](https://doi.org/10.1109/TEC.2006.875468)
- 2 [28] Uzunoglu M, Onar OC, Alam MS. Dynamic behavior of PEM FCPPs under various  
3 load conditions and voltage stability analysis for stand-alone residential applications. J  
4 Power Sources 2007;168(1):240-50. <https://doi.org/10.1016/j.jpowsour.2007.02.045>
- 5 [29] Yalcinoz T. A Dynamic Model and Analysis of PEM Fuel Cells for an Electric  
6 Bicycle. In: 2018 IEEE International Conference on Environment and Electrical  
7 Engineering and 2018 IEEE Industrial and Commercial Power Systems Europe  
8 (EEEIC/I&CPS Europe) 2018 Jun 12; Europe. IEEE; 2018. p. 1-5.  
9 [10.1109/EEEIC.2018.8493821](https://doi.org/10.1109/EEEIC.2018.8493821)
- 10 [30] Kundu A, Jang JH, Gil JH, Jung CR, Lee HR, Kim SH, et al. Micro-fuel cells—current  
11 development and applications. J Power Sources 2007;170(1):67-78.  
12 <https://doi.org/10.1016/j.jpowsour.2007.03.066>
- 13 [31] Benchouia NE, Derghal A, Mahmah B, Madi B, Khochemane L, Aoul EH. An  
14 adaptive fuzzy logic controller (AFLC) for PEMFC fuel cell. Int J Hydrogen Energy  
15 2015;40(39):13806-19. <https://doi.org/10.1016/j.ijhydene.2015.05.189>
- 16 [32] Hemi H, Ghouili J, Cheriti A. A real time fuzzy logic power management strategy for  
17 a fuel cell vehicle. Energy Convers Manag 2014;80:63-70.  
18 <https://doi.org/10.1016/j.enconman.2013.12.040>
- 19 [33] Sakhare A, Davari A, Feliachi A. Fuzzy logic control of fuel cell for stand-alone and  
20 grid connection. J Power Sources 2004;135(1-2):165-76.  
21 <https://doi.org/10.1016/j.jpowsour.2004.04.013>
- 22 [34] Ou K, Yuan WW, Choi M, Yang S, Kim YB. Performance increase for an open-

- 1 cathode PEM fuel cell with humidity and temperature control. Int J Hydrogen Energy  
2 2017;42(50):29852-62. <https://doi.org/10.1016/j.ijhydene.2017.10.087>
- 3 [35] Morner SO, Klein SA. Experimental evaluation of the dynamic behavior of an air-  
4 breathing fuel cell stack. J Sol Energy Eng 2001;123(3):225-31.  
5 <https://doi.org/10.1115/1.1385202>
- 6 [36] Yalcinoz T, Alam MS. Dynamic modeling and simulation of air-breathing proton  
7 exchange membrane fuel cell. J Power Sources 2008;182(1):168-74.  
8 <https://doi.org/10.1016/j.jpowsour.2008.03.076>
- 9 [37] Alnejaili T, Drid S, Mehdi D, Chrifi-Alaoui L, Belarbi R, Hamdouni A. Dynamic  
10 control and advanced load management of a stand-alone hybrid renewable power  
11 system for remote housing. Energy Convers Manag 2015;105:377-92.  
12 <https://doi.org/10.1016/j.enconman.2015.07.080>
- 13 [38] O'Hayre R, Cha SW, Colella W, Prinz FB. Fuel cell fundamentals. 3rd ed. New Jersey:  
14 John Wiley & Sons; 2016.
- 15 [39] Sone Y, Ekdunge P, Simonsson D. Proton conductivity of Nafion 117 as measured by  
16 a four-electrode AC impedance method. J Electrochem Soc 1996;143(4):1254.  
17 [10.1149/1.1836625](https://doi.org/10.1149/1.1836625)
- 18 [40] Springer TE, Zawodzinski TA, Gottesfeld S. Polymer electrolyte fuel cell model. J  
19 Electrochem Soc 1991;138(8):2334. [10.1149/1.2085971](https://doi.org/10.1149/1.2085971)
- 20 [41] Kim HI, Cho CY, Nam JH, Shin D, Chung TY. A simple dynamic model for polymer  
21 electrolyte membrane fuel cell (PEMFC) power modules: Parameter estimation and  
22 model prediction. Int J Hydrogen Energy 2010;35(8):3656-63.

1 <https://doi.org/10.1016/j.ijhydene.2010.02.002>

2 [42] Alhazmi N, Ismail MS, Ingham DB, Hughes KJ, Ma L, Pourkashanian M. The in-  
3 plane thermal conductivity and the contact resistance of the components of the  
4 membrane electrode assembly in proton exchange membrane fuel cells. J Power  
5 Sources 2013;241:136-45. <https://doi.org/10.1016/j.jpowsour.2013.04.100>

6 [43] Alhazmi N, Ingham DB, Ismail MS, Hughes K, Ma L, Pourkashanian M. The through-  
7 plane thermal conductivity and the contact resistance of the components of the  
8 membrane electrode assembly and gas diffusion layer in proton exchange membrane  
9 fuel cells. J Power Sources 2014 ;270:59-67.  
10 <https://doi.org/10.1016/j.jpowsour.2014.07.082>

11